JOURNAL OF NATURAL PRODUCTS

Article

pubs.acs.org/jnp

Can Small Chemical Modifications of Natural Pan-inhibitors Modulate the Biological Selectivity? The Case of Curcumin Prenylated Derivatives Acting as HDAC or mPGES-1 Inhibitors

Mehrdad Iranshahi,[†,‡] Maria Giovanna Chini,[§,‡] Milena Masullo,[§] Amirhossein Sahebkar,[†] Azita Javidnia,[⊥] Mahsa Chitsazian Yazdi,[†] Carlo Pergola,[∥] Andreas Koeberle,[∥] Oliver Werz,[∥] Cosimo Pizza,[§] Stefania Terracciano,[§] Sonia Piacente,[*,§] and Giuseppe Bifulco[*,§]

[†]Biotechnology Research Center and School of Pharmacy, Mashhad University of Medical Sciences, Vakil Abad Boulevard, Opposite Mellat Park, 91775-1365 Mashhad, Iran

[§]Department of Pharmacy, University of Salerno, Via Giovanni Paolo II 132, 84084 Fisciano (SA), Italy

[⊥]Department of Medicinal Chemistry, Faculty of Pharmacy, Tehran University of Medical Sciences, Enghlab Street, 14155-6559 Tehran, Iran

[∥]Institute of Pharmacy, Friedrich Schiller University Jena, Philosophenweg 14, 07743 Jena, Germany

Supporting Information

ABSTRACT: Curcumin, or diferuloylmethane, a polyphenolic molecule isolated from the rhizome of *Curcuma longa*, is reported to modulate multiple molecular targets involved in cancer and inflammatory processes. On the basis of its pan-inhibitory characteristics, here we show that simple chemical modifications of the curcumin scaffold can regulate its biological selectivity. In particular, the curcumin scaffold was modified with three types of substituents at positions C-1, C-8, and/or C-8′ [C_5 (isopentenyl, **5**−**8**), C_{10} (geranyl, **9**−**12**), and C_{15} (farnesyl, **13**, **14**)] in order to make these molecules more selective than the parent compound toward two specific targets: histone deacetylase (HDAC) and microsomal prostaglandin E_2 synthase-1 (mPGES-1). From combined in silico and in vitro analyses, three selective inhibitors by proper substitution at position 8 were revealed. Compound **13** has improved HDAC inhibitory activity and selectivity with respect to the parent compound, while **5** and **9** block the mPGES-1 enzyme. We hypothesize about the covalent interaction of curcumin, **5**, and **9** with the mPGES-1 binding site.

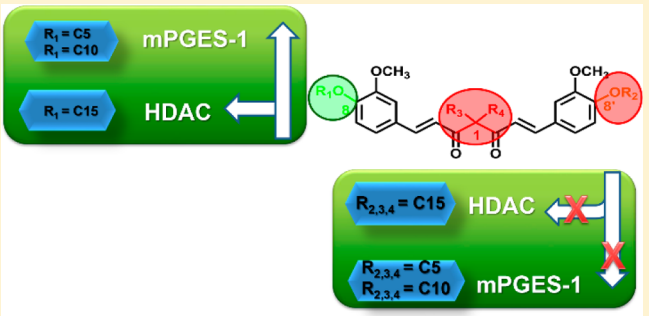

The isolation and characterization of active natural products (NPs) have produced a multitude of derivatives useful both in therapy and in the study of physiological mechanisms. In clinical applications, in fact, analogues and/or derivatives of NPs have often been used in order to modulate the pharmacokinetic or pharmacodynamic properties of lead compounds. Some representative examples involve the alkaloid family; for example, nalorphine (**1**), with an allyl group as R_1, antagonizes the effects of morphine (**2**, from *Papaver somniferum*), while ethylmorphine (**3**), with an ethyl group as R_2, causes a complete drop of analgesic activity (Figure 1), showing that small and simple modifications of a parent compound can influence its pharmacological activity.

Several examples of chemical modifications of the curcumin scaffold have been reported in order to modify the selectivity, potency, and the bioavailability[1,2] of this pan-inhibitor. Recent results[3,4] have shown that the prenyl groups at C-9 are able to modulate the biological selectivity of curcumin (**4**, Figure 2). Here we describe the case of this polyphenolic molecule and its prenylated congeners (**5**−**14**, Figure 2) that selectively inhibit two targets involved in cancer and inflammatory processes: histone deacetylase (HDAC) and microsomal prostaglandin E_2 synthase-1 (mPGES-1).

Curcumin (**4**), a polyphenolic molecule isolated from the rhizome of *Curcuma longa* (Zingiberaceae), has a profile of a safe drug, and it has been used in the treatment of inflammatory, cancer, neurodegenerative, cardiovascular, and metabolic diseases, modulating multiple pathways. In particular, curcumin directly inhibits some biological targets (e.g., transcription factors, protein kinases) or indirectly up-regulates (e.g., JNK, p53, DN5) or down-regulates (TNF, EGFR)[5] numerous others crucial for several inflammatory and cancer pathologies[5−8] by noncovalent hydrophobic and hydrogen-bonding interactions.[9,10] Owing to its multitude of actions,[6,10] curcumin has several clinical applications, and for these reasons this natural product and its derivatives are currently involved in

Received: May 5, 2015

DOI: 10.1021/acs.jnatprod.5b00700
J. Nat. Prod. XXXX, XXX, XXX−XXX

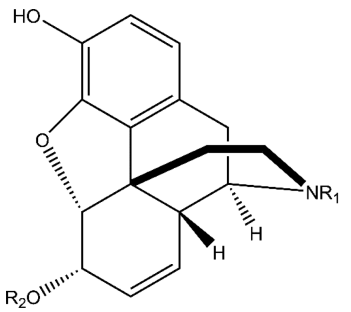

R_1 = 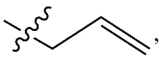 , R_2 =H, nalorphine (**1**)

R_1 = Me, R_2 =H, morphine (**2**)

R_1 =Me, R_2 =Et, ethylmorphine (**3**)

Figure 1. Examples of morphine analogues whose activity is influenced by small chemical substitutions on the scaffold.

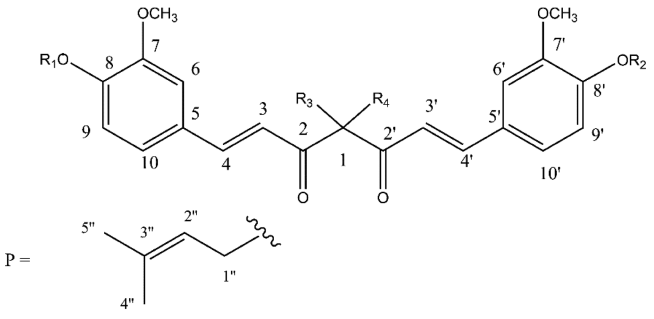

	R_1	R_2	R_3	R_4
4	H	H	H	H
5	P	H	H	H
6	P	P	H	H
7	P	P	P	H
8	P	P	P	P
9	G	H	H	H
10	G	G	H	H
11	G	G	G	H
12	G	G	G	G
13	F	H	H	H
14	F	F	H	H

Figure 2. Chemical structure of curcumin (**4**) and its derivatives (**5**–**14**).

many clinical trials.[2] Thus, it would be crucial to clarify, at the molecular level, the selectivity of curcumin toward a specific target, in order to develop new and more active and selective analogues. To prove this hypothesis, we investigated two targets directly inhibited by curcumin[11,12] and which were exhaustively studied: HDAC[13−18] and mPGES-1.[19−23]

The first class of enzyme is involved in the epigenetic modifications[24,25] linked to cancer development and progression. The impact of curcumin (**4**, Figure 2) on these epigenetic mechanisms[26,27] has been evaluated and has revealed its ability to inhibit HDAC in a more effective manner with respect to the well-known HDACi, such as valproic acid and sodium butyrate,[2] appearing as a new member of HDAC inhibitors (HDACi).[13−18,28−31] In particular, when combined with HDACi, curcumin suppresses tumor progression proteins and cell migration in vitro and blocks tumor growth and metastasis in vivo.[32]

On the other hand, microsomal prostaglandin E_2 synthase-1 enzyme, belonging to the membrane-associated proteins involved in the eicosanoid and glutathione metabolism (MAPEG) family, has emerged as an attractive target for the development of novel anti-inflammatory and anticancer drugs.[33] This enzyme is responsible, via the arachidonic acid cascade, for the conversion of COX-derived unstable peroxide PGH_2 into PGE_2[34] without affecting the constitutive prostaglandins implicated in physiological functions. It is overexpressed in several inflammatory disorders,[35−39] and for this reason, the identification of new mPGES-1 inhibitors is essential for the development of safer drugs devoid of classical NSAID side effects. Closely related to the inflammatory diseases, mPGES-1 is involved in the pathogenesis of different cancer forms and in induction of angiogenesis.[40] However, despite several inhibitors being identified,[41−43] only a few of them exhibit in vivo anticancer and anti-inflammatory[44−46] properties.

The recent resolution of the human X-ray structures of mPGES-1 from 2013[47] to date[48] and of the high-resolution X-ray structure of human mPGES-1 in lipidic mesophase in 2014[49] in complex with a potent inhibitor have represented attractive starting points for the rational design of new mPGES-1 inhibitors.

Collectively these considerations prompted an evaluation of the influence of simple prenyl groups[50,51] at C-8 and/or C-8′ and C-1 on modulation of biological selectivity of the parent compound on HDACs and mPGES-1 of some synthetically accessible curcumin derivatives (**5**–**14**). In particular, we have performed a computational study of the affinities of **4**–**14**, identifying **5** and **9** as selective mPGES-1 inhibitors, and **13**, which inhibits HDACs and also shows an increment of potency with respect to curcumin. Interestingly, because the α,β-unsaturated β-diketo moiety of curcumin covalently interacts with protein thiols[9,10,52,53] through a Michael[54] reaction and mPGES-1 has a glutathione (GSH) cofactor in the catalytic binding site, we have envisaged a covalent interaction between **4**, **5**, and **9** with the GSH cofactor.

DOI: 10.1021/acs.jnatprod.5b00700
J. Nat. Prod. XXXX, XXX, XXX−XXX

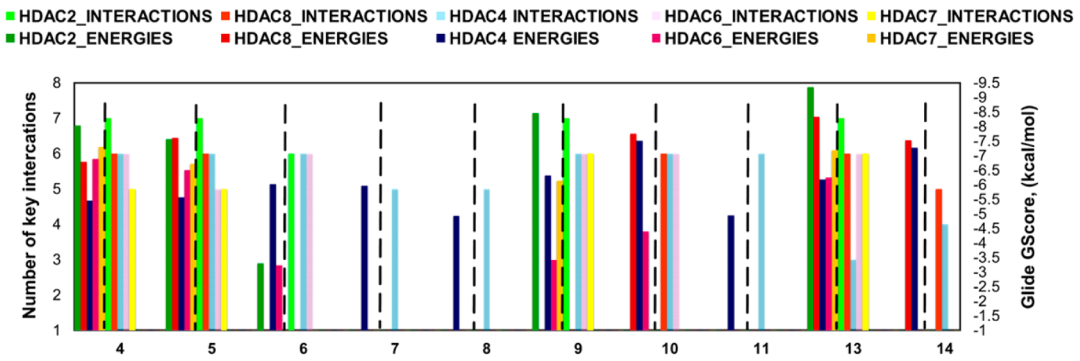

Figure 3. Glide GScore (dark bars at the left of the dotted black line) and number of key interactions (light bars at the right of the dotted black line) of **4**−**11**, **13**, and **14** for HDACs. For the calculated activity the interactions with the following amino acids were considered discriminant: (a) Leu276, Phe144, Tyr209, the $\pi-\pi$ interaction with His183 and Phe210, and the coordination (mono- or bidentate mode) with Zn^{2+} for HDAC2; (b) Phe152, Tyr306, His143, His180, the $\pi-\pi$ interaction with Trp141, and the coordination (mono- or bidentate mode) with Zn^{2+} for HDAC8; (c) Tyr170, Phe168, His159, His158, the $\pi-\pi$ interaction with Phe227, and the coordination (mono- or bidentate mode) with Zn^{2+} for HDAC4; (d) Phe140, Arg126, Gly301, the $\pi-\pi$ interaction with Phe200 and His171, and the coordination of Zn^{2+} for HDAC6; (e) Phe738, His669, Pro542, Glu543, the $\pi-\pi$ interaction with His709, and the coordination of Zn^{2+} for HDAC7.

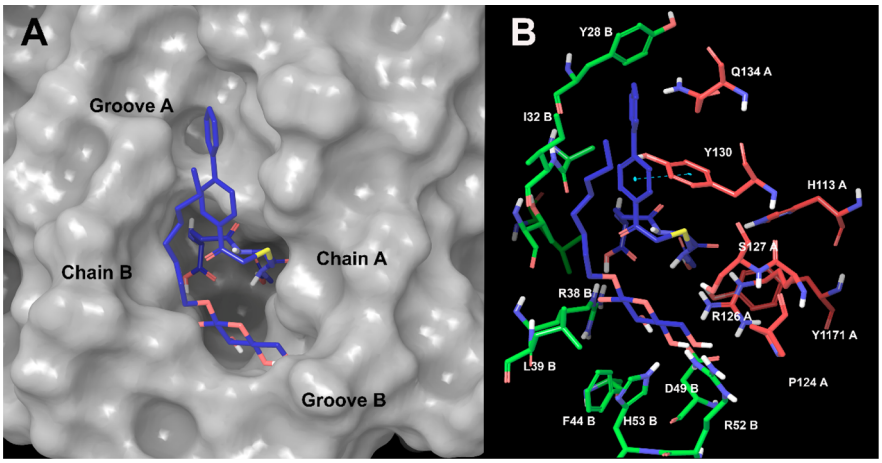

Figure 4. Three-dimensional model of cocrystallized molecules (GSH analogue and β-octyl glucoside (dark blue sticks), PDB code: 4AL1) in the receptor binding site of mPGES-1. In panel B the crucial amino acids of the mPGES-1 receptor are depicted as sticks colored by chain (A, red; B, green). The π-stacking interaction is represented by a cyan dotted line.

RESULTS AND DISCUSSION

Docking Studies. A small set of readily synthesizable curcumin analogues, **5**−**14** (Figure 2), were designed gradually substituting the curcumin scaffold at C-8, C-8′ (R_1 and R_2), and C-1 (R_3 and R_4) with simple prenylated moieties [C_5 (isopentenyl), C_{10} (geranyl), and C_{15} (farnesyl)]. These compounds were used as suitable case studies to test the influence of simple chemical modifications of the curcumin scaffold on the regulation of its biological selectivity. In order to prove the hypothesis of this work, computational studies were performed by molecular docking (Glide software version 6.1, standard and extra precision level)[55−58] on these targets, to disclose the structural basis for modulation of the bioactivity of **4**.

For computational studies, the X-ray and homology model structures[14] of HDACs of class I (HDAC1, 2, 3, and 8)[59−62] and class II (HDAC4, 6, and 7)[14,63,64] and the recent experimental structure of mPGES-1[47] were used. From a qualitative point of view, the ability of compounds to bind the targets, expressed by a Glide score (kcal/mol) and by the number of key interactions established with the ligand binding sites of HDACs and mPGES-1,[14,20,22,23,47−49,66] was considered. For the HDACs, the coordination of the Zn^{2+} ion and the interactions with the receptor counterparts have been considered essential for the simulated inhibition,[14,65,66] and, from the analysis of the computational data (Figure 3), **4**, together with the molecules with substitution at C-8 (**5**, **9**, and **13**), showed the most interesting results. In particular, they are able to chelate the zinc ion in a bidentate (for HDAC2) and monodentate fashion (HDAC8, HDAC4, HDAC6, HDAC7) and to arrange the R_1 substituent in the cavities of the HDAC's surface. On the other hand, the compounds with R_1 and R_2 substitution groups (**6**, **10**, **14**) retain weak calculated affinities for HDACs (Figure 3), while **7**, **8**, and **11** (R_3 and R_4 at C-1) are able to interact only with HDAC4 due to the different shape of the residues at the rim of the catalytic channel. None of the compounds are able to chelate the zinc ion of HDAC1 and HDAC3, probably because of the dimension of the catalytic channel[14,59] and the shape of the protein surface,[14] which hinder the access of the zinc-chelating moiety. Finally, full substitution with geranyl moieties at R_1-R_4 of **12** leads to complete inactivity.

Concerning the mPGES-1 receptor, the 3D model of curcumin (**4**) and its analogues (**5**−**14**) with the X-ray structure of the target[47] are reported for the first time. As

DOI: 10.1021/acs.jnatprod.5b00700
J. Nat. Prod. XXXX, XXX, XXX−XXX

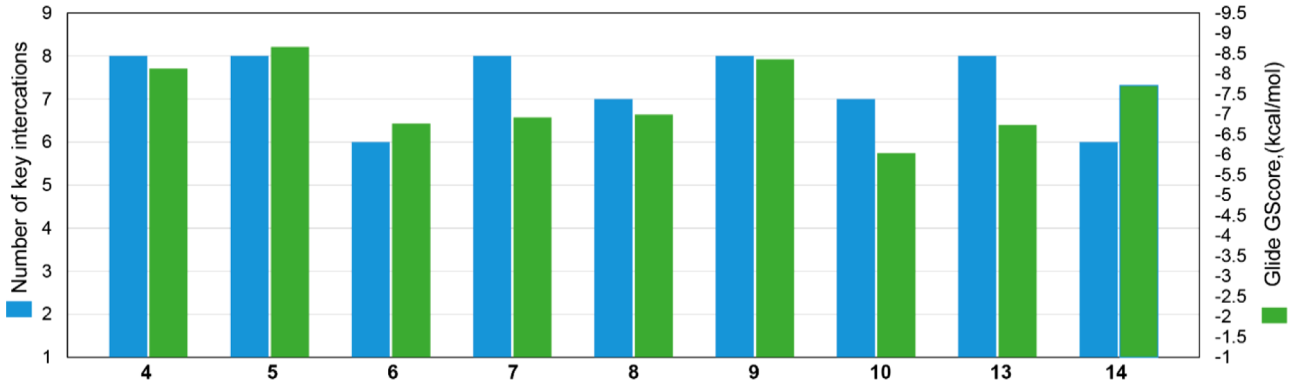

Figure 5. Glide GScore and number of key interactions ($Tyr130_{chain\ A}$, $Ser127_{chain\ A}$, $Asp49_{chain\ B}$, $Gln134_{chain\ A}$, $His53_{chain\ B}$, $Phe44_{chain\ B}$, $Thr131_{chain\ A}$, $Tyr28_{chain\ B}$) of **4**–**10**, **13**, and **14** for mPGES-1.

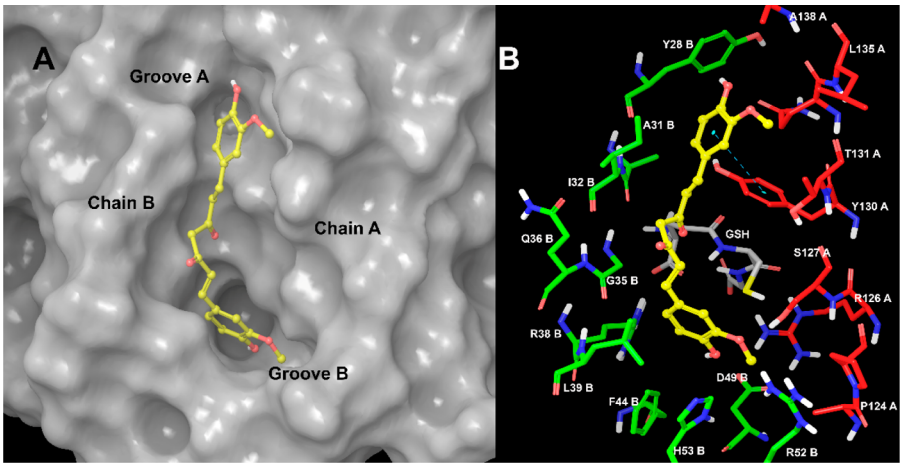

Figure 6. Three-dimensional models of the interactions of curcumin (**4**, yellow sticks) in the mPGES-1 binding site. In panel B the crucial amino acids of the mPGES-1 receptor are depicted as sticks colored by chain (A, red; B, green). The π-stacking interaction is represented by a cyan dotted line.

Scheme 1. General Synthetic Procedure and Chemical Structures of Synthesized Curcumin Derivatives

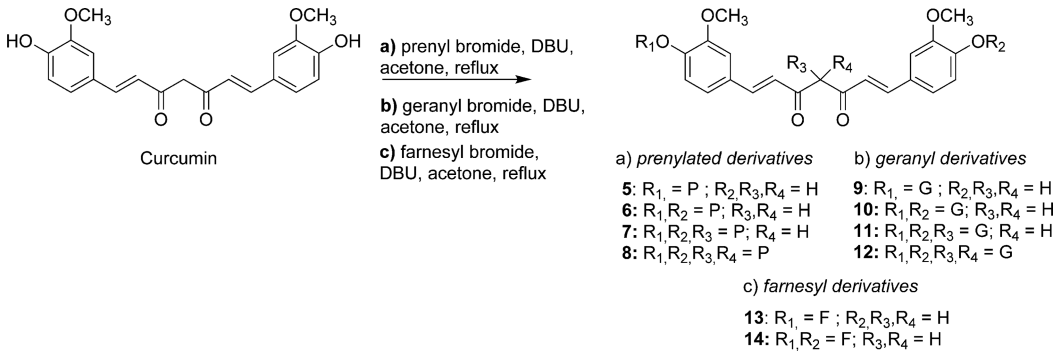

reported by Geschwindner et al.,[47] the mPGES-1 active site is divisible into the cofactor (GSH) and substrate (PGH_2) binding site, and it includes the N-terminal (helices II and IV) and C-terminal (helix I) parts and an adjacent monomer cytoplasmic domain. The pattern of binding is well represented by the cocrystallized structure of mPGES-1 with the GSH analogue [L-γ-glutamyl-*S*-(2-biphenyl-4-yl-2-oxoethyl)-L-cysteinylglycine] and a β-octyl glucoside moiety (Figure 4), disclosing several key interactions for a rational design of a substrate site inhibitor.

Docking calculations between curcumin (**4**) and analogues **5**–**14** and mPGES-1, in order to verify the presence of some key interactions with the receptor counterpart (Figure 5), were performed:[47−49] (a) π–π with $Tyr130_{chain\ A}$, indicative of a good accommodation within the GSH binding site;[20] (b) effective contacts (van der Waals and polar interactions) with $Ser127_{chain\ A}$, a key residue involved in PGH_2 recognition, and with $Asp49_{chain\ B}$, $Gln134_{chain\ A}$, $His53_{chain\ B}$, $Phe44_{chain\ B}$, $Thr131_{chain\ A}$, and $Tyr28_{chain\ B}$, belonging to the binding groove.[20,22,23]

Thus, curcumin interacts in the enzyme active site with the same set of residues observed for the GSH analogue and β-octyl glucoside (Figure 6), strongly supporting the significance of the docking results. The two phenyl rings of curcumin (Figure 6)

DOI: 10.1021/acs.jnatprod.5b00700
J. Nat. Prod. XXXX, XXX, XXX−XXX

Table 1. Individual and Total Yields of Prenylated Curcumin Analogues (5−14)

molar ratio	5	6	7	8	9	10	11	12	13	14	total yield
curcumin:1-bromo-3-methyl-2-butene:DBU											
1:1:1	24	10									34
1:3:3	19	24	16	1							60
2:24:21			37	38							84
curcumin:geranyl bromide:DBU											
1:1:1					15	38					53
2:24:21					15	36	8	19			78
curcumin:farnesyl bromide:DBU											
1:1:1									21	5	26

interact with grooves A ($Gln134_{Chain\ A}$, $Tyr130_{Chain\ A}$, and $Ile32_{Chain\ B}$) and B ($Leu39_{Chain\ B}$, $Phe44_{Chain\ B}$, $His53_{Chain\ B}$, and $Asp49_{Chain\ B}$) on the receptor molecular surface, and it establishes further contacts with $Gly35_{Chain\ B}$, $Arg38_{Chain\ B}$, and the GSH cofactor of chain A.

Comparing the results for the two targets, **5**, **9**, and **13** represent the most active derivatives of **4**, showing C-8 as the important determinant for the modulation of the predicted biological selectivity and activity.

In order to verify the above in silico results, the synthesis and biological evaluation of compounds **5**−**14** were next pursued.

Synthesis. Compounds **5**−**14** were synthesized by dissolution of curcumin in acetone and subsequent addition of 1-bromo-3-methyl-2-butene (2 mmol, 240 μL) and DBU (1,8-diazabicyclo[5.4.0]undec-7-ene).[67] By using different molar ratios (excess of 1-bromo-3-methyl-2-butene and DBU) and temperature (reflux) compounds **5**−**14** were obtained and successively purified by column chromatography on silica gel and preparative TLC (Scheme 1). Precumins I−IV (**5**−**8**) are characterized by the presence of one prenyl moiety at C-8 (precumin I), two prenyl moieties at C-8 and C-8′ (precumin II), three prenyl moieties at positions C-1, C-8, and C-8′ (precumin III), and four prenyl moieties, two at C-1 and the other two at C-8 and C-8′ (precumin IV).

In order to synthesize geranyl derivatives (**9**−**12**) of curcumin, named gercumins I−IV, curcumin was dissolved in acetone and reacted with different molar ratios of geranyl bromide in the presence of DBU. The resulting compounds, purified by column chromatography on silica gel, showed the same geranyl pattern of substitution with respect to **5**−**8**. Similarly, for the synthesis of farcumins I (**13**) and II (**14**), curcumin, dissolved in acetone, was treated with farnesyl bromide in the presence of DBU. The purified compounds were curcumin derivatives characterized by a farnesyl moiety at C-8 (farcumin I) and at C-8 and C-8′ (farcumin II). The percentage yields of compounds **5**−**14** are reported in Table 1. The structures of compounds **5**−**14** have been confirmed by 1D (^1H and ^{13}C) and 2D NMR (HSQC, HMBC, and COSY) experiments along with ESIMS analysis.

HDAC Biological Results. To test HDAC inhibitory activity, curcumin (**4**) and compounds **5**−**14** have been screened in vitro by using a fluorescence-based assay in HeLa cell nuclear extracts (see Experimental Section) in 10-dose IC_{50} mode with 2-fold serial dilution starting at 3.333 mM. Trichostatin A (TSA), a well-established HDAC inhibitor, was used as control compound in a 10-dose IC_{50} with 3-fold serial dilution starting at 10 μM. The IC_{50} values for tested compounds are reported in Table 2.

Among the screened compounds, farcumin I (**13**) was found to be the most active, with an IC_{50} value of 84.2 μM with respect to curcumin (187 μM). Compounds **10**, **14**, and curcumin showed comparable activity (Table 2), and precumin I (**5**) displayed weaker activity (IC_{50} = 5.62 mM). Precumins III (**7**) and IV (**8**) were ineffective for HDAC inhibition (data not shown).

Table 2. In Vitro HDAC Inhibitory Activity of Tested Compounds 4−14

compound	IC_{50}
curcumin (**4**)	187 μM
5	5.62 mM
6	347 μM
7	[a]
8	[a]
9	495 μM
10	188 μM
11	217 μM
12	786 μM
13	84.2 μM
14	122 μM
trichostatin A	1.42 nM

[a]Empty cells indicate no inhibition or absence of compound activity that could not be fit to an IC_{50} curve.

mPGES-1 Biological Results. In order to study compounds **5**−**14** for inhibition of mPGES-1, a cell-free activity assay was used, where the substrate PGH_2 is converted by mPGES-1 in microsomes from IL-1β-activated A549 cells to PGE_2.[68] Curcumin (**4**) potently inhibited mPGES-1 activity with an IC_{50} value of 0.22 μM, which is in agreement with a previous finding.[12] The monoisopentenylated **5** and the monogeranylated **9** showed potent inhibition of mPGES-1, although the IC_{50} values (0.93 and 1.02 μM, respectively) are comparable to **4**. Similarly, derivatives carrying two to four isopentenyl (**6**−**8**) or geranyl (**10**−**12**) residues as well as one or two farnesyl moieties (**13**, **14**) were bioactive, but the potency was further impaired and the IC_{50} values were determined in the range 2−8 μM.

Selectivity Profile. The aforementioned results have permitted the creation of a basic SAR profile of the most promising molecules with respect to parent compound **4** ($IC_{50\text{-for-mPGES-1}}$ = 0.22 μM, $IC_{50\text{-for-HDACs}}$ = 187 μM), which show remarkable inhibition in the low μM range for mPGES-1 (**5**, IC_{50} = 0.93 μM, and **9**, IC_{50} = 1.02 μM), and in vitro interesting HDAC (**13**, $IC_{50\text{-for-HDACs}}$ = 84.2 μM) inhibitory activity. From the computational analysis, C-8 of the curcumin scaffold (Figures 3 and 5) was identified as a modification point able to modulate the biological activity of the parent pan-inhibitor compound, and this result is consistent with biological data, which have confirmed the hypothesis, and that in

DOI: 10.1021/acs.jnatprod.5b00700
J. Nat. Prod. XXXX, XXX, XXX−XXX

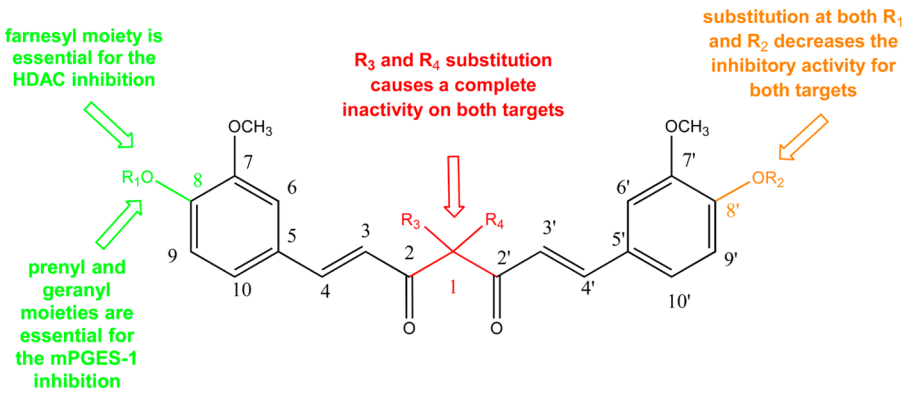

Figure 7. SAR summary profile for **5**−**14**.

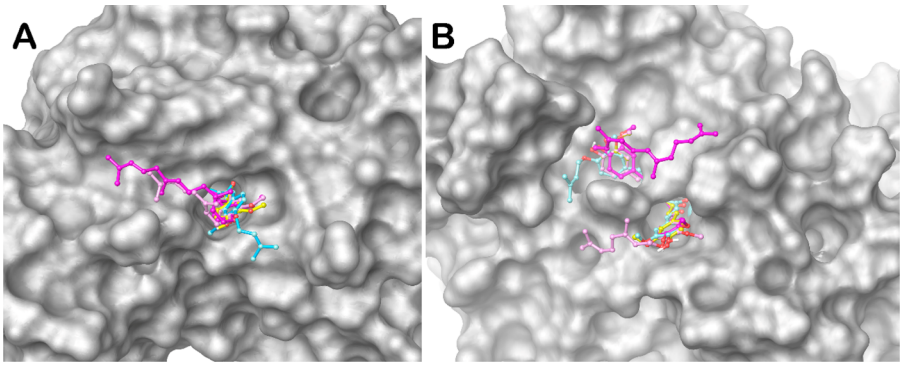

Figure 8. Three-dimensional models of **4** (yellow), **5** (light blue), **9** (light pink), and **13** (fuchsia) in complex with HDAC2 (class I) (panel A) and HDAC6 (class II) (panel B).

particular the length of the chain at C-8 mainly influences the bioselectivity of curcumin analogues (Figure 7).

The 3D models of curcumin and of the most promising candidates **5**, **9**, and **13** in complex with one representative receptor for each class of HDACs (HDAC2 and HDAC6) (Figures 8−10) were illustrated to identify the main features of new potential curcumin-based HDACi and to summarize the critical points for the modulation of the biological activity on HDACs shown by these compounds.

Concerning HDAC2, the contacts with Leu276, Phe144, and Tyr209, the $\pi-\pi$ interaction with His183 and Phe210, and the coordination (mono- or bidentate mode) with the metal atom were considered as key interactions. As shown above (Table 2), the substitution at C-8 of curcumin (**4**) with increasing alkyl group size, yielding **5**, **9**, and **13**, influences the inhibitory activity on HDAC. In fact, the better biological profile observed for compound **13** is due to the larger farnesyl moiety, which is able to establish peculiar hydrophobic contacts with the macromolecule surface (namely, with Gln31, Glu103, Gly30, and Pro106) with respect to **4**, **5**, and **9** (Figure 9).

As observed for HDAC2 by computational analysis, the gain derived from the contacts of the R_1 alkyl chain of **13** with HDAC6 relating to the other compounds seems to be the driving force of the target−ligand complexes. In addition to the key contacts with Phe140, Arg126, and Gly301, the $\pi-\pi$ interaction with Phe200 and His171, and the coordination of Zn^{2+}, **13** is also interacting with Asp169, Asp267, His130, and Phe86 (Figure 10).

On the other hand, compounds with multiple prenyl, geranyl, and farnesyl substitutions (**6**−**8**, **10**, **11**, and **14**) show a decrease of calculated and experimental potency with respect to **13**. The in silico analysis of compounds **6**−**8**, **10**, **11**, and **14**, i.e., curcumin analogues with three substitutions (**7** and **11**) at the other possible positions (Figure 2), revealed that, even if they are able to weakly interact with HDAC4, they have reduced biological activity due to the steric hindrance responsible for reducing the optimal contacts with the other HDAC isoforms. Only compound **14**, possessing two farnesyl groups as R_1 and R_2, acts as a weak inhibitor, proving the alkyl chain with 15 atoms as the preferred substituent on the curcumin skeleton for the HDAC inhibition.

From the analysis of binding modes of **5**−**14** in comparison with **4** in the mPGES-1 active site, the molecules with one substitution at R_1 (Figure 11) maintain a similar pattern of contacts, in particular the hydrophobic contacts with groove B and the key $\pi-\pi$ interaction with $Tyr130_{ChainB}$.

In addition, **5**, **9**, and **13** increase their interactions in groove A, making further interactions with $Val29_{Chain\ B}$ and $Ile25_{Chain\ B}$, and, $Leu142_{Chain\ A}$ is involved in hydrophobic contact with **9** and **13**. On the other hand, the increased chain length of the substituent at C-8 of **9** and **13** permits interaction with $Cys137_{Chain\ A}$ and $Ile33_{Chain\ B}$, respectively. Moreover, the presence of the R_2, R_3, and R_4 alkyl chains hampers the interactions with grooves A and B and produces the loss of the key contacts with the mPGES-1 binding site, namely, with $Arg126_{Chain\ A}$, $Arg38_{Chain\ B}$, and $Phe44_{Chain\ B}$ for **6** and with $Asp49_{Chain\ B}$ for **6** and **8** (see Figure 5 and Supporting Information). Comparing the binding mode of **5** with respect to **6**−**8**, which shows the prenylated moieties at R_1, R_2, R_3, and R_4, respectively, it is evident how the alkyl chain R_2 causes the shifting of aromatic rings in grooves A and B (Figure S39, Supporting Information), and the substituents at R_3 and R_4,

DOI: 10.1021/acs.jnatprod.5b00700
J. Nat. Prod. XXXX, XXX, XXX−XXX

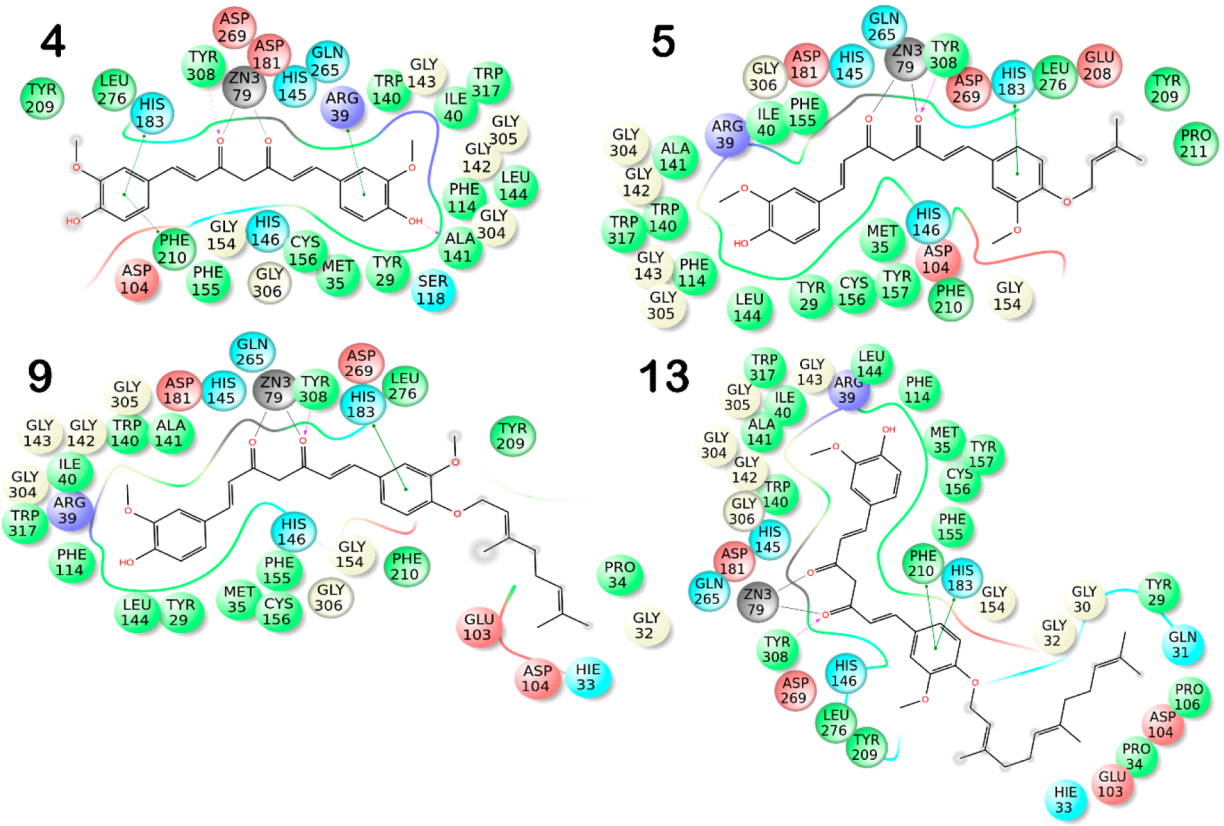

Figure 9. 2D interaction diagrams of **4**, **5**, **9**, and **13** with the HDAC2 binding site. The hydrophobic residues are displayed in green, the polar residues are displayed in light blue, the positively charged residues are in violet, and the negatively charged residues are in red. H-bonds are indicated as pink dotted arrows (side chain) and continuous (backbone) pink arrows, and $\pi-\pi$ interactions are depicted as continuous green arrows.

protruding toward the solvent/membrane region, interact in an unfavorable manner.

Moreover, as anticipated above, on the bases of the biological data, the possibility that curcumin, **5**, and **9** establish a covalent interaction with the GSH cofactor in the mPGES-1 catalytic site was also evaluated. In particular, the covalent docking module[69] of the Schrödinger suite was used to obtain a binding mode between the polyphenolic molecules and the enzyme, simulating a Michael addition, where the SH of GSH attacks the α,β-unsaturated β-diketo moiety.[9,10,52−54] Curcumin (**4**) and its congeners (**5** and **9**) are able to bind the GSH (Figure 12), keeping the fundamental interactions with the mPGES-1 binding site, maintaining quite similar binding modes with respect to the noncovalent ones (see above).

In all three models the nonsubstituted aromatic portion interacts with the amino acids of groove B (Ans46$_{\text{Chain B}}$, Asp49$_{\text{Chain B}}$, Phe 44$_{\text{Chain B}}$, etc.) in the same manner, while the other part of the molecules in the compound-GSH-mPGES-1 complex interact with groove A, like the GSH analogue cocrystallized with the enzyme (Figure 4). In particular, 8-OH of **4** forms a hydrogen bond with Gln134$_{\text{Chain A}}$ (Figure 12a), while the 8′-OH of **5** (Figure 12b) and **9** (Figure 12c) interacts with Asp49$_{\text{Chain B}}$. Moreover, the phenyl ring substituted with prenyl moiety (Figure 12b) of **5** retains a $\pi-\pi$ interaction with Tyr130$_{\text{Chain A}}$, while **9** (Figure 12c) establishs a cation$-\pi$ interaction with Arg126$_{\text{Chain A}}$.

The alkyl groups at C-8 show hydrophobic interactions with Ile25$_{\text{Chain B}}$, Val29$_{\text{Chain B}}$, and Leu142$_{\text{Chain B}}$, demonstrating from the structural point of view the possibility of covalent inhibition; in fact, further substitutions with prenylated moieties at R_2, R_3, and R_4 could restrain the formation of the covalent complexes.

In summary, by means of the docking studies, the qualitative predictions have proved that the different size of substituent groups at C-8 can modulate the biological selectivity of curcumin. In fact, these results confirm that the topology and the size of alkyl groups are the most important determinants for biological selectivity and activity of these curcumin scaffold-based inhibitors. In particular, the increased C-8 chain-length of **13** allows favorable interactions with the HDAC receptor surfaces, while it causes a great structural difference with respect to the dimension of the natural PGH_2 substrate of mPGES-1. On the other hand, the dimension of the alkyl chains of **5** and **9** represents the maximum length allowed to retain a biological activity on this MAPEG member receptor, and it is compatible with the covalent hypothesis inhibition.

EXPERIMENTAL SECTION

General Experimental Procedures. Melting points were determined on a Sanyo Gallenkamp apparatus. NMR experiments were performed on a Bruker DRX-600 spectrometer (Bruker BioSpinGmBH, Rheinstetten, Germany) equipped with a Bruker 5 mm TCI CryoProbe at 300 K. All 2D NMR spectra were acquired in $CDCl_3$ (99.95%, Sigma-Aldrich), and standard pulse sequences and phase cycling were used for DQF-COSY, HSQC, and HMBC spectra. The NMR data were processed using Xwinnmr software. Exact masses were measured by an AB SCIEX Voyager DE mass spectrometer equipped with a 337 nm laser and delay extraction and operated in positive-ion reflector mode. Samples were analyzed by MALDI-TOF mass spectrometry. A mixture of analyte solution and α-cyano-4-hydroxycinnamic acid (Sigma) was applied to the metallic sample plate

DOI: 10.1021/acs.jnatprod.5b00700
J. Nat. Prod. XXXX, XXX, XXX−XXX

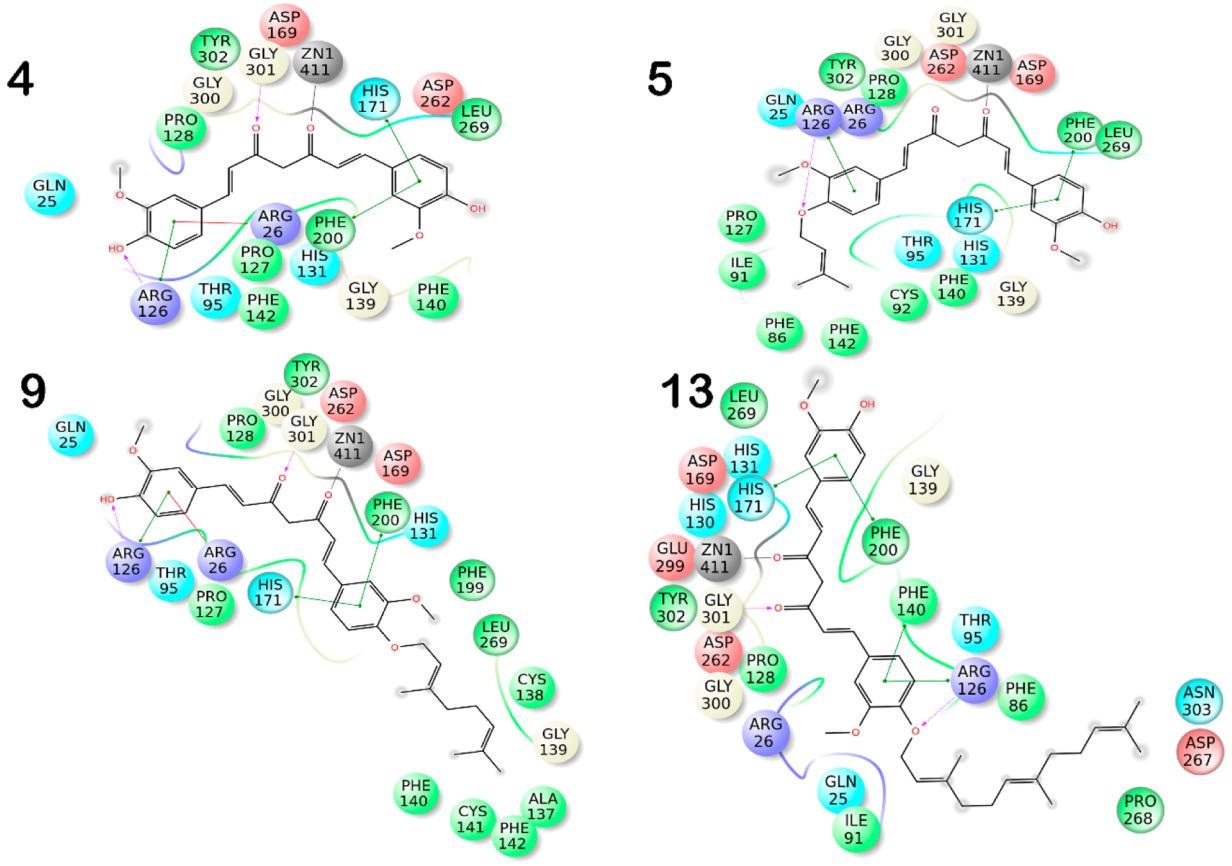

Figure 10. 2D interaction diagrams of **4**, **5**, **9**, and **13** with the HDAC6 binding site. The hydrophobic residues are displayed in green, the polar residues are displayed in light blue, the positively charged residues are in violet, and the negatively charged residues are in red. H-bonds are indicated as pink dotted arrows (side chain) and continuous (backbone) pink arrows. $\pi-\pi$ and cation$-\pi$ interactions are depicted as continuous green and red arrows, respectively.

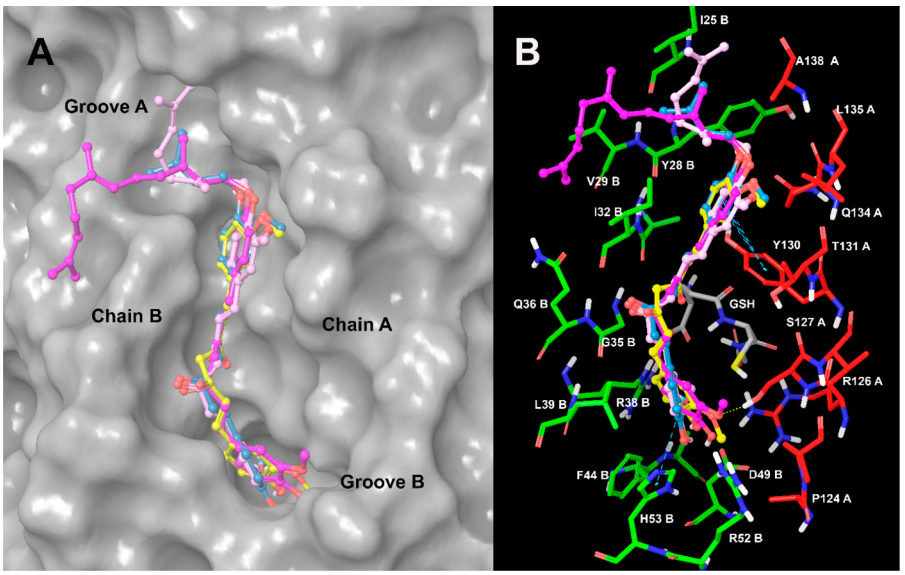

Figure 11. Three-dimensional models of **4** (yellow), **5** (light blue), **9** (light pink), and **13** (fuchsia) with mPGES-1 binding site. In panel B the crucial amino acids of the mPGES-1 receptor are depicted as sticks colored by chain (A, red; B, green). The π-stacking interaction and hydrogen bonds are represented by cyan and yellow dotted lines, respectively.

and dried. Mass calibration was performed with the ions from adrenocorticotropic hormone (ACTH) fragment 18−39 human at 2465.1989 Da and α-cyano-4-hydroxycinnamic acid at 190.0504 Da as internal standard. Column chromatography was conducted with silica gel (Mesh 230−400, 0.040−0.063 mm, Merck).

Curcumin Preparation. Curcumin 65−70% (product code #C 1386) was purchased from Sigma-Aldrich. Curcumin of 65−70% purity was further purified[70] by silica gel column chromatography, using CH_2Cl_2 as eluent. The isolated curcumin was crystallized from MeOH/H_2O (9:1), as orange needles. Physicochemical characteristics

DOI: 10.1021/acs.jnatprod.5b00700
J. Nat. Prod. XXXX, XXX, XXX−XXX

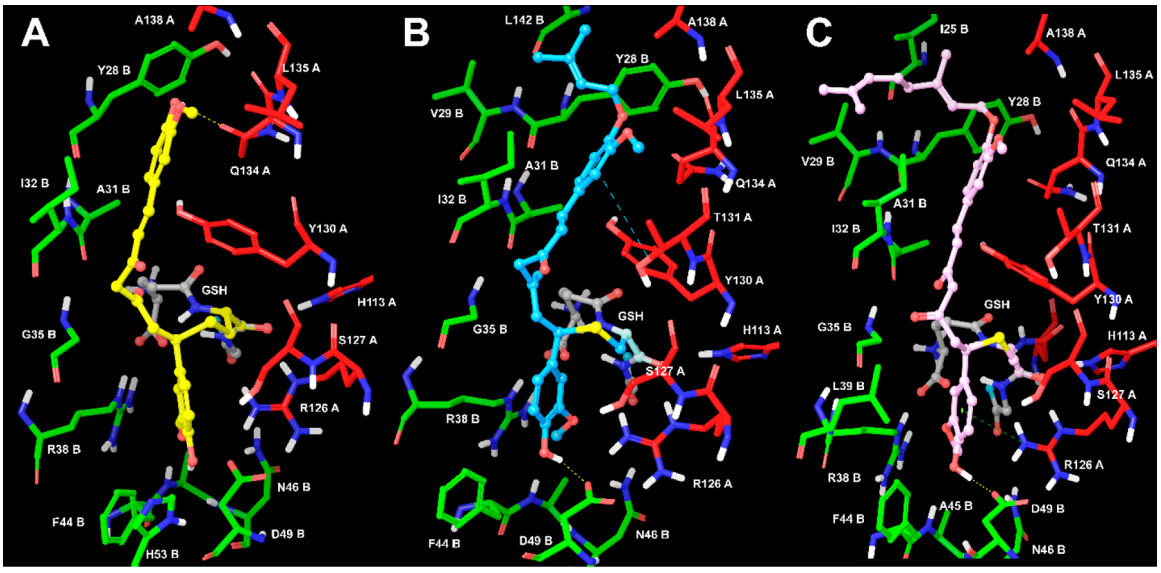

Figure 12. Three-dimensional models of covalent complexes between **4** (yellow sticks), **5** (light blue sticks), **9** (light pink sticks), and cofactor GSH (stick colored by atom type) of mPGES-1. The crucial amino acids of the mPGES-1 receptor are depicted as sticks colored by chain (A, green; B, red; C, blue). The π-stacking interaction, cation$-\pi$, and hydrogen bonds are represented by cyan, green, and yellow dotted lines, respectively.

Table 3. ^{1}H NMR and ^{13}C NMR Data for Precumins I–IV (5–8) (600 MHz, δ ppm, in $CDCl_3$)

	5		6		7		8	
position	δ_H (J in Hz)	δ_C	δ_H (J in Hz)	δ_C	δ_H (J in Hz)	δ_C	δ_H (J in Hz)	δ_C
1	5.82, s	102.4	5.83, s	102.2		111.9		70.0
2, 2′		184.5, 184.4		184.3		184.3		198.5
3, 3′	6.48, 6.51, d (16.0)	123.1, 123.0	6.52, d (16.0)	122.9	6.88, d (15.5)	125.6	6.69, d (15.5)	120.8
4, 4′	7.58, 7.61, d (16.0)	141.8, 141.7	7.63, d (16.0)	141.5	7.67, d (15.5)	141.8	7.68, d (15.5)	145.0
5, 5′		129.3, 129.0		129.3		129.6		128.4
6, 6′	7.06, 7.08, d (2.0)	111.0, 111.1	7.09, d (2.0)	110.8	7.08, d (1.5)	110.7	7.02, d (2.0)	111.1
7, 7′		148.4, 149.0		150.8		150.4		150.8
8, 8′		151.3, 146.1		151.7		151.8		152.2
9, 9′	6.87, 6.93, d (8.0)	113.6, 115.8	6.90, d (8.5)	113.6	6.86, d (8.5)	113.6	6.84, d (8.5)	113.5
10, 10′	7.12, 7.11, dd (8.0, 2.0)	123.8, 123.6	7.13, dd (8.5, 2.0)	123.5	7.12, dd (8.5, 1.5)	123.5	7.12, dd (8.5, 2.0)	124.4
OCH_3	3.93, s	56.9	3.93, s	56.9	3.91, s	56.9	3.91, s	57.2
	prenyl moiety at C-8		prenyl moieties at C-8,8′		prenyl moieties at C-8,8′		prenyl moieties at C-8,8′	
1″	4.65, d (7.0)	66.9	4.65, d (7.0)	66.7	4.62, d (7.0)	66.7	4.62, d (7.0)	66.7
2″	5.53, brt (7.0)	120.4	5.53, brt (7.0)	120.4	5.52, brt (7.0)	120.4	5.50, brt (7.0)	120.4
3″		139.4		139.6		139.6		139.6
4″	1.76, s	19.4	1.76, s	19.4	1.75, s,	19.4	1.76, s,	19.4
5″	1.80, s	27.1	1.80, s	27.1	1.78, s	27.1	1.79, s	27.1
					prenyl moiety at C-1		prenyl moieties at C-1	
1‴					3.28 (2H), d (6.7)	27.1	2.79 (2H), d (6.7)	30.2
2‴					5.16, t (6.7)	119.8	4.88, t (6.7)	119.3
3‴						133.0		136.5
4‴					1.75, s	19.4,	1.60, s	19.2,
5‴					1.85, s	27.4	1.68, s	27.4

were in agreement with literature data.[70] TLC experiments showed that curcumin was completely free of demethoxycurcumin and bisdemethoxycurcumin.

Curcumin Analogues with C_5 (Prenyl) Side Chain(s): Precumins I–IV (5–8). For the synthesis of precumins I (**5**) and II (**6**), curcumin (2 mmol, 736 mg) was dissolved in acetone (50 mL). Then, 1-bromo-3-methyl-2-butene (2 mmol, 240 μL) and DBU (2 mmol, 300 μL) were added, and the mixture was refluxed for 2 h at 37 °C. Precumins I and II were isolated by decantation of the reaction mixture with distilled H_2O (75 mL) and EtOAc (75 mL), followed by separation and solvent evaporation of the organic phase. The products were purified by silica gel column chromatography using a 40 cm × 5 cm column and a petroleum ether/acetone/MeOH (5:1:0.1) mixture as eluent. The fractions (80 mL each) were analyzed by TLC (using a mixture of petroleum ether/acetone/MeOH, 2.5:1:0.1). Precumin II (**6**) was further purified by preparative TLC using a petroleum ether/acetone/MeOH (2.5:1:0.1 v/v) system as eluent. For the synthesis of precumin III (**7**), a similar procedure was applied using curcumin (2 mmol, 736 mg), 1-bromo-3-methyl-2-butene (6 mmol, 720 μL), and DBU (6 mmol, 900 μL), followed by purification by silica gel column chromatography (55 cm × 5 cm). Precumin III (**7**) was further purified by preparative TLC using a petroleum ether/acetone/MeOH (2.5:1:0.1 v/v) system as eluent. For the synthesis of precumin IV (**8**), curcumin (2 mmol, 736 mg) was dissolved in acetone (50 mL). Then, 1-bromo-3-methyl-2-butene (24 mmol, 2880 μL) and DBU (21 mmol,

DOI: 10.1021/acs.jnatprod.5b00700
J. Nat. Prod. XXXX, XXX, XXX−XXX

Table 4. ^{1}H NMR and ^{13}C NMR Data for Gercumins I–IV (9–12) (600 MHz, δ ppm, in $CDCl_3$)

	9		10		11		12	
	δ_H (J in Hz)	δ_C	δ_H (J in Hz)	δ_C	δ_H (J in Hz)	δ_C	δ_H (J in Hz)	δ_C
1	5.82, s	101.1	5.85, s	101.4		111.9		68.3
2, 2′		183.4, 183.3		182.6		184.3		197.4
3, 3′	6.51, 6.48, d (16.0)	122.1, 122.2	6.52, d (16.0)	122.6	6.88, d (15.5)	125.6	6.65 d (16.0)	119.9
4, 4′	7.61, 7.59, d (16.0)	140.7, 140.5	7.63, d (16.0)	140.9	7.67, d (15.5)	141.8	7.66 d (16.0)	143.9
5, 5′		127.9, 128.9		127.4		129.6		127.1
6, 6′	7.06, 7.08, d (1.8)	109.7, 110.0	7.11, d (1.8)	110.2	7.06, d (1.5)	110.8	6.99 d (1.8)	110.3
7, 7′		149.5, 146.8		149.8		150.4		149.6
8, 8′		150.8, 146.7		150.3		151.8		150.9
9, 9′	6.88, 6.93, d (8.3)	112.7, 115.2	6.90, d (8.0)	113.0	6.87, d (8.5)	113.6	6.82 d (8.3)	112.7
10, 10′	7.12, 7.11, dd (8.3, 1.8)	122.5, 122.8	7.13, dd (8.0, 1.8)	123.0	7.11, dd (8.5, 1.5)	123.5	7.08 dd (8.3, 1.8)	123.5
OCH_3	3.93, 3.95, s	56.1	3.95 s	56.1	3.91, s	55.9	3.86 s	56.1
	geranyl moiety at C-8		geranyl moieties at C-8,8′		geranyl moieties at C-8,8′		geranyl moieties at C-8,8′	
1″	4.67, d (6.3)	66.4	4.69, d (6.3)	66.3	4.66, d (6.6)	66.2	4.63 d (7.0)	66.0
2″	5.51, t (6.3)	119.2	5.53, t (6.3)	119.5	5.50, d (6.6)	119.3	5.46 t (7.0)	119.2
3″		141.4		141.4		141.2		141.3
4″	2.08, (2H) m	39.6	2.10, (2H) m	39.6	2.06, (2H) m	39.5	2.04 (2H) m	39.7
5″	2.12, (2H) m	26.4	2.14, (2H) m	26.4	2.11, (2H) m	26.2	2.09 (2H) m	26.4
6″	5.09, t (6.8)	123.8	5.11, t (6.8)	123.8	5.08, t (6.8)	123.9	5.03 t (6.8)	124.1
7″		131.7		131.4		131.8		131.3
8″	1.68, s	26.1	1.70, s	26.2	1.66, s	26.0	1.63 s	26.0
9″	1.61, s	18.0	1.63, s	18.3	1.59, s	17.7	1.62, s	16.6
10″	1.75, s	17.0	1.77, s	17.3	1.74, s	16.9	1.70, s	16.9
					geranyl moiety at C-1		geranyl moieties at C-1	
1‴					3.25, (2H) d (6.5)	26.1	2.77, (2H) d (7.0)	29.1
2‴					5.16, t (6.5)	118.9	4.89, t (7.0)	118.3
3‴						141.8		138.3
4‴					2.06, (2H) m	39.9	1.95, (2H) m	40.2
5‴					2.11, (2H) m	26.6	1.99, (2H) m	26.5
6‴					5.08, (6.8)	124.2	5.04, t (6.8)	124.1
7‴						131.8		131.4
8‴					1.55, s	26.1	1.63, s	26.0
9‴					1.56, s	17.6	1.56, s	17.7
10‴					1.58, s	17.9	1.54, s	17.7

3150 μL) were added, and the mixture was refluxed for 3.5 h and then sonicated for 1 h at 30 °C.

After isolation and solvent evaporation, the products were purified by silica gel column chromatography (35 cm × 3 cm). Eleven fractions (each 50 mL) were collected and analyzed by TLC using petroleum ether/EtOAc (different ratios).

Curcumin Analogues with C_{10} (Geranyl) Side Chain(s): Gercumins I–IV (9–12). Curcumin (2 mmol, 736 mg) was dissolved in acetone (50 mL) and treated with geranyl bromide (2 mmol, 400 μL) in the presence of DBU (2 mmol, 300 μL). The mixture was refluxed for 2.5 h at 37 °C. After the reaction was completed (confirmed by TLC), the products were isolated by decantation of the reaction mixture with distilled H_2O (75 mL) and EtOAc (75 mL). After separation and solvent evaporation of the organic phase, the products were purified by silica gel column chromatography using a mixture of petroleum ether/acetone/MeOH (5:1:0.1 v/v) as eluent. The fractions (80 mL each) were analyzed by TLC [petroleum ether/acetone/MeOH (2.5:1:0.1 v/v)]. Synthesis of gercumins III (**11**) and IV (**12**) was carried out using the above procedure with the following molar ratios: curcumin (1 mmol, 368 mg), geranyl bromide (12 mmol, 2400 μL), and DBU (10.5 mmol, 1575 μL). Isolation and purification of products was performed by decantation with H_2O (60 mL) and EtOAc (60 mL), followed by silica gel column (60 cm × 5 cm) chromatography using a mixture of petroleum ether/acetone/MeOH (10:1:2.5 v/v) as eluent. The fractions (30 mL each) were analyzed by TLC [petroleum ether/acetone/MeOH (5:1:2.5 v/v)].

Curcumin Analogues with C_{15} (Farnesyl) Side Chain: Farcumins I and II (13 and 14). Curcumin (2 mmol, 736 mg) was dissolved in acetone (50 mL) and treated with farnesyl bromide (purity: 95%; 2 mmol, 532 μL) in the presence of DBU (2 mmol, 300 μL). The mixture was refluxed for 2 h at 37 °C. Isolation and purification steps were performed as described for precumins. After the reaction was completed (confirmed by TLC), the products were isolated by decantation of the reaction mixture with distilled H_2O (75 mL) and EtOAc (75 mL). After separation and solvent evaporation of the organic phase, the products were purified by silica gel column chromatography, using petroleum ether/acetone/MeOH (5:1:0.1 v/v) as eluent.

*Precumin I (**5**):* viscous, brownish liquid; yield is reported in Table 1; IR (KBr) ν_{max} 3360 (br OH), 2925 (CH), 1685 (C═O), 1665 (C═C) cm^{-1}; ^{1}H NMR (600 MHz, $CDCl_3$) and ^{13}C NMR (150 MHz, $CDCl_3$) data are reported in Table 3; ESIMS m/z 437.2 $[M + H]^+$; HR-MALDI-TOFMS $[M + H]^+$ m/z 437.1968 (calcd for $C_{26}H_{29}O_6$, 437.1964).

*Precumin II (**6**):* orange crystals; yield is reported in Table 1; mp 120–121 °C; 3440 (br OH), 2934 (CH), 1650 (C═C); ^{1}H NMR (600 MHz, $CDCl_3$) and ^{13}C NMR (150 MHz, $CDCl_3$) data are reported in Table 3; ESIMS m/z 505.3 $[M + H]^+$; HR-MALDI-TOFMS $[M + H]^+$ m/z 505.2595 (calcd for $C_{31}H_{37}O_6$, 505.2590).

*Precumin III (**7**):* orange crystals; yield is reported in Table 1; mp 143–144 °C; 3448 (br OH), 2934 (CH), 1640 (C═C); ^{1}H NMR (600 MHz, $CDCl_3$) and ^{13}C NMR (150 MHz, $CDCl_3$) data are reported in Table 3; ESIMS m/z 573.3 $[M + H]^+$; HR-MALDI-TOFMS $[M + H]^+$ m/z 573.3218 (calcd for $C_{36}H_{45}O_6$, 573.3216).

*Precumin IV (**8**):* pale yellow crystals; yield is reported in Table 1; mp 58–60 °C; 3455 (br OH), 2945 (CH), 1648 (C═C); ^{1}H NMR

DOI: 10.1021/acs.jnatprod.5b00700
J. Nat. Prod. XXXX, XXX, XXX–XXX

(600 MHz, $CDCl_3$) and ^{13}C NMR (150 MHz, $CDCl_3$) data are reported in Table 3; ESIMS m/z 641.4 $[M + H]^+$; HR-MALDI-TOFMS $[M + H]^+$ m/z 641.3847 (calcd for $C_{41}H_{53}O_6$, 641.3842).

*Gercumin I (**9**):* viscous, brownish liquid; yield is reported in Table 1; 3445 (br OH), 2938 (CH), 1650 (C=C); ^1H NMR (600 MHz, $CDCl_3$) and ^{13}C NMR (150 MHz, $CDCl_3$) data are reported in Table 4; ESIMS m/z 505.3 $[M + H]^+$; HR-MALDI-TOFMS $[M + H]^+$ m/z 505.2595 (calcd for $C_{31}H_{37}O_6$, 505.2590).

*Gercumin II (**10**):* yellow crystals; yield is reported in Table 1; mp 62−64 °C; 3440 (br OH), 2934 (CH), 1650 (C=C); ^1H NMR (600 MHz, $CDCl_3$) and ^{13}C NMR (150 MHz, $CDCl_3$) data are reported in Table 4; ESIMS m/z 641.4 $[M + H]^+$; HR-MALDI-TOFMS $[M + H]^+$ m/z 641.3845 (calcd for $C_{41}H_{53}O_6$, 641.3842).

*Gercumin III (**11**):* viscous, brownish liquid; yield is reported in Table 1; 3450 (br OH), 2940 (CH), 1645 (C=C); ^1H NMR (600 MHz, $CDCl_3$) and ^{13}C NMR (150 MHz, $CDCl_3$) data are reported in Table 4; ESIMS m/z 777.5 $[M + H]^+$; HR-MALDI-TOFMS $[M + H]^+$ m/z 777.5097 (calcd for $C_{51}H_{69}O_6$, 777.5094).

*Gercumin IV (**12**):* viscous, brownish liquid; yield is reported in Table 1; 3455 (br OH), 2936 (CH), 1655 (C=C); ^1H NMR (600 MHz, $CDCl_3$) and ^{13}C NMR (150 MHz, $CDCl_3$) data are reported in Table 4; ESIMS m/z 913.6 $[M + H]^+$; HR-MALDI-TOFMS $[M + H]^+$ m/z 912.6270 (calcd for $C_{61}H_{84}O_6$, 912.6268).

*Farcumin I (**13**):* viscous, brownish liquid; yield is reported in Table 1; 3452 (br OH), 2936 (CH), 1640 (C=C); ^1H NMR (600 MHz, $CDCl_3$) and ^{13}C NMR (150 MHz, $CDCl_3$) data are reported in Table 5; ESIMS m/z 573.3 $[M + H]^+$; HR-MALDI-TOFMS $[M + H]^+$ m/z 573.3219 (calcd for $C_{36}H_{45}O_6$, 573.3216).

*Farcumin II (**14**):* viscous, brownish liquid; yield is reported in Table 1; 3453 (br OH), 2938 (CH), 1648 (C=C); ^1H NMR (600 MHz, $CDCl_3$) and ^{13}C NMR (150 MHz, $CDCl_3$) data are reported in Table 5; ESIMS m/z 777.5 $[M + H]^+$; HR-MALDI-TOFMS $[M + H]^+$ m/z 777.5098 (calcd for $C_{51}H_{69}O_6$, 777.5094).

Table 5. ^1H NMR and ^{13}C NMR Data for Farcumins I and II (13 and 14) (600 MHz, δ ppm, in $CDCl_3$)

	13		14	
position	δ_H (J in Hz)	δ_C	δ_H (J in Hz)	δ_C
1	5.83 s	102.2	5.85, s	102.9
2, 2′		184.3, 184.2		184.8
3, 3′	6.52, 6.48, d (16.0)	122.7, 122.9	6.51, d (15.7)	124.9
4, 4′	7.63, 7.60 d (16.0)	141.5, 141.3	7.63, d (15.7)	141.5
5, 5′		129.5, 129.0		129.3
6, 6′	7.07, 7.10, d (1.5)	110.7, 109.8	7.12, d (1.5)	111.0
7, 7′		150.5, 148.1		150.8
8, 8′		151.5, 146.8		151.7
9, 9′	6.89, 6.95, d (8.3)	113.5, 115.8	6.90, d (8.3)	113.6
10, 10′	7.13, 7.15, d (8.3)	123.4, 123.6	7.14, dd (8.3, 1.5)	123.5
OCH_3	3.95, 3.96, s	56.9	3.96, s	57.1
	farnesyl moiety at C-8		farnesyl moieties at C-8,8′	
1″	4.69 (2H), d (6.3)	66.9	4.70 (2H), d (6.3)	66.9
2″	5.53, t (6.3)	120.2	5.54, t (6.3)	120.2
3″		142.7		142.7
4″	2.11 (2H), m	40.7	2.11 (2H), m	40.8
5″	2.16 (2H), m	27.5	2.16 (2H), m	27.4
6″	5.12, t (6.8)	124.9	5.12, t (6.8)	124.9
7″		136.9		136.9
8″	2.00 (2H), m	40.8	1.98 (2H), m	40.8
9″	2.08 (2H), m	28.0	2.08 (2H), m	28.0
10″	5.12, t (6.8)	124.9	5.12, t (6.8)	124.9
11″		132.9		132.9
12″	1.63, s	18.1	1.63, s	18.1
13″	1.71, s	27.1	1.71, s	27.1
14″	1.63, s	18.1	1.63, s	18.1
15″	1.78, s	18.1	1.78, s	18.1

In Vitro Biological Assays. Inhibition of HDAC activity in HeLa nuclear extracts by curcumin (**4**) and **5**−**14** was measured using the HDAC fluorimetric assay on nuclear extract substrate BML-KI104 Fluor de Lys by Reaction Biology Corp. (Malvern, PA, USA). HDAC activities were evaluated by testing the compounds in 10-dose IC_{50} mode with 2-fold serial dilution starting at 3.333 mM. HDAC control compound trichostatin A was tested in a 10-dose IC_{50} with 3-fold serial dilution starting at 10 μM. Determination of fluorescence of tested compounds was performed to ensure that the samples gave no interference in the assay. All compounds exhibited no fluorescent background except compounds **8**, **11**, and **12**, which showed a weak fluorescent background at 3.33 and 1.11 mM.

Preparations of A549 cells and determination of mPGES-1 activity were performed as described by Koeberle et al.[68] In brief, cells were treated with 2 ng/mL IL-1β for 72 h at 37 °C, 5% CO_2, harvested, sonicated, and homogenized (homogenization buffer: 0.1 M K_3PO_4 buffer, pH 7.4, 1 mM PMSF, 60 μg/mL STI, 1 μg/mL leupeptin, 2.5 mM glutathione, and 250 mM sucrose). The homogenate was centrifuged at 10000g for 10 min and 174000g for 1 h at 4 °C, the resulting pellet (microsomal fraction) was resuspended in 1 mL of homogenization buffer, and the total protein concentration was determined. Microsomal membranes were diluted in K_3PO_4 buffer (0.1 M, pH 7.4) containing 2.5 mM glutathione. Test compounds or vehicle was added, and after 15 min at 4 °C reaction (100 μL total volume) was initiated by addition of 20 μM PGH_2. After 1 min at 4 °C, the reaction was terminated using stop solution (100 μL; 40 mM $FeCl_2$, 80 mM citric acid, and 10 μM 11β-PGE_2 as internal standard), followed by solid-phase extraction and analysis of PGE_2 by HPLC.

Computational Details. The chemical structures of investigated compounds were built with Maestro[71] (version 9.6) Build Panel, then processed with LigPrep[72] at a pH of 7.4 ± 1.0, and finally minimized using OPLS 2005 force field (Schrödinger Suite 2013).

Protein 3D models were prepared using the Schrödinger Protein Preparation Wizard (Maestro version 9.6).[71] Calculations were performed using the Glide software package (standard precision (SP) and extra precision (XP) modes, version 6.1, Schrödinger package)[55−58] in order to determine the binding mode of compounds **4**−**14** into the HDAC and mPGES-1 cavities. The receptor grids were generated focused on sites of pharmacological interest for each protein (Table S1 in the Supporting Information). The sampling step was set to expanded sampling mode (4 times), keeping 10 000 ligand poses for the initial phase of docking, followed by 800 ligand poses selected for energy minimization. A maximum number of 15 (SP mode) and 15 (XP mode) output structures were saved for each ligand, with a scaling factor of 0.8 related to van der Waals radii with a partial charge cutoff of 0.15. A postdocking optimization of the obtained docking outputs for each SP and XP mode was performed, accounting for a maximum of five poses based on a 0.5 kcal/mol rejection cutoff for the obtained minimized poses.

The covalent docking between **4**, **5**, **9**, and the cofactor GSH of mPGES-1 was done using the covalent docking[69] protocol of the Schrödinger suite. In particular, the Michael addition was chosen as reaction type, between the α,β-unsaturated β-diketo moiety (identified as the ligand functional group after the Ligfilter step)[73] and the cofactor GSH (reactive receptor residue). Covalent docking experiments were performed generating a receptor grid focused on the mPGES-1 binding site, considering the residues close to the cofactor GSH as the centroid of the docking box (7.80 (x), −9.26 (y), −8.16 (z)), with inner box and outer box dimensions of 14 × 14 × 14 Å and 52 × 52 × 52 Å, respectively. For scoring the poses, the option of the calculate affinity score using Glide was used, where a noncovalent binding affinity score using the results of Glide docking and a score-in-place calculation using the final docked pose is calculated. The average of the two GlideScore values is used for the affinity. Docking results and illustrations of the 3D and 2D models were generated using Maestro version 9.6.[71]

DOI: 10.1021/acs.jnatprod.5b00700
J. Nat. Prod. XXXX, XXX, XXX−XXX

■ ASSOCIATED CONTENT

Supporting Information

The Supporting Information is available free of charge on the ACS Publications website at DOI: 10.1021/acs.jnatprod.5b00700.

NMR spectra of **5**−**14**, computational details (PDB codes, grid details), and 2D interactions diagram of **4**−**14** with HDAC and mPGES-1 binding sites (PDF)

■ AUTHOR INFORMATION

Corresponding Authors

*For S. Piacente, Phone: +39-089-969763. Fax: +39-089-969602. E-mail: piacente@unisa.it.

*For G. Bifulco, Phone: +39-089-969741. Fax: +39-089-969602. E-mail: bifulco@unisa.it.

Author Contributions

‡M. Iranshahi and M. G. Chini contributed equally to this work.

Notes

The authors declare no competing financial interest.

■ ACKNOWLEDGMENTS

Financial support by Associazione Italiana Ricerca sul Cancro (AIRC) Grant IG 2012−IG_12777−Giuseppe Bifulco is gratefully acknowledged.

■ REFERENCES

(1) Anand, P.; Thomas, S. G.; Kunnumakkara, A. B.; Sundaram, C.; Harikumar, K. B.; Sung, B.; Tharakan, S. T.; Misra, K.; Priyadarsini, I. K.; Rajasekharan, K. N.; Aggarwal, B. B. *Biochem. Pharmacol.* **2008**, *76*, 1590−1611.

(2) Fan, X.; Zhang, C.; Liu, D.-b.; Yan, J.; Liang, H.-p. *Curr. Pharm. Des.* **2013**, *19*, 2011−2031.

(3) Minassi, A.; Sanchez-Duffhues, G.; Antonio Collado, J.; Munoz, E.; Appendino, G. *J. Nat. Prod.* **2013**, *76*, 1105−1112.

(4) Koeberle, A.; Munoz, E.; Appendino, G. B.; Minassi, A.; Pace, S.; Rossi, A.; Weinigel, C.; Barz, D.; Sautebin, L.; Caprioglio, D.; Collado, J. A.; Werz, O. *J. Med. Chem.* **2014**, *57*, 5638−5648.

(5) Aggarwal, B. B.; Sung, B. *Trends Pharmacol. Sci.* **2009**, *30*, 85−94.

(6) Teiten, M.-H.; Eifes, S.; Dicato, M.; Diederich, M. *Toxins* **2010**, *2*, 128−162.

(7) Coussens, L. M.; Werb, Z. *Nature* **2002**, *420*, 860−867.

(8) Wang, S.-L.; Li, Y.; Wen, Y.; Chen, Y.-F.; Na, L.-X.; Li, S.-T.; Sun, C.-H. *Biomed. Environ. Sci.* **2009**, *22*, 32−39.

(9) Gupta, S. C.; Prasad, S.; Kim, J. H.; Patchva, S.; Webb, L. J.; Priyadarsini, I. K.; Aggarwal, B. B. *Nat. Prod. Rep.* **2011**, *28*, 1937−1955.

(10) Priyadarsini, K. I. *Curr. Pharm. Des.* **2013**, *19*, 2093−2100.

(11) Bora-Tatar, G.; Dayangac-Erden, D.; Demir, A. S.; Dalkara, S.; Yelekci, K.; Erdem-Yurter, H. *Bioorg. Med. Chem.* **2009**, *17*, 5219−5228.

(12) Koeberle, A.; Northoff, H.; Werz, O. *Mol. Cancer Ther.* **2009**, *8*, 2348−2355.

(13) Chini, M. G.; Terracciano, S.; Riccio, R.; Bifulco, G.; Ciao, R.; Gaeta, C.; Troisi, F.; Neri, P. *Org. Lett.* **2010**, *12*, 5382−5385.

(14) Di Micco, S.; Chini, M. G.; Terracciano, S.; Bruno, I.; Riccio, R.; Bifulco, G. *Bioorg. Med. Chem.* **2013**, *21*, 3795−3807.

(15) Terracciano, S.; Chini, M. G.; Riccio, R.; Bruno, I.; Bifulco, G. *ChemMedChem* **2012**, *7*, 694−702.

(16) Terracciano, S.; Chini, M. G.; Bifulco, G.; D'Amico, E.; Marzocco, S.; Riccio, R.; Bruno, I. *Tetrahedron* **2010**, *66*, 2520−2528.

(17) Grolla, A. A.; Podesta, V.; Chini, M. G.; Di Micco, S.; Vallario, A.; Genazzani, A. A.; Canonico, P. L.; Bifulco, G.; Tron, G. C.; Sorba, G.; Pirali, T. *J. Med. Chem.* **2009**, *52*, 2776−2785.

(18) Maulucci, N.; Chini, M. G.; Di Micco, S.; Izzo, I.; Cafaro, E.; Russo, A.; Gallinari, P.; Paolini, C.; Nardi, M. C.; Casapullo, A.; Riccio, R.; Bifulco, G.; De Riccardis, F. *J. Am. Chem. Soc.* **2007**, *129*, 3007−3012.

(19) Chini, M. G.; De Simone, R.; Bruno, I.; Riccio, R.; Dehm, F.; Weinigel, C.; Barz, D.; Werz, O.; Bifulco, G. *Eur. J. Med. Chem.* **2012**, *54*, 311−323.

(20) Lauro, G.; Strocchia, M.; Terracciano, S.; Bruno, I.; Fischer, K.; Pergola, C.; Werz, O.; Riccio, R.; Bifulco, G. *Eur. J. Med. Chem.* **2014**, *80*, 407−415.

(21) De Simone, R.; Chini, M. G.; Bruno, I.; Riccio, R.; Mueller, D.; Werz, O.; Bifulco, G. *J. Med. Chem.* **2011**, *54*, 1565−1575.

(22) Chini, M. G.; Ferroni, C.; Cantone, V.; Dambruoso, P.; Varchi, G.; Pepe, A.; Fischer, K.; Pergola, C.; Werz, O.; Bruno, I.; Riccio, R.; Bifulco, G. *MedChemComm* **2015**, *6*, 75−79.

(23) Terracciano, S.; Lauro, G.; Strocchia, M.; Fischer, K.; Werz, O.; Riccio, R.; Bruno, I.; Bifulco, G. *ACS Med. Chem. Lett.* **2015**, *6*, 187−191.

(24) Kristensen, L. S.; Nielsen, H. M.; Hansen, L. L. *Eur. J. Pharmacol.* **2009**, *625*, 131−142.

(25) Ropero, S.; Esteller, M. *Mol. Oncol.* **2007**, *1*, 19−25.

(26) Reuter, S.; Gupta, S. C.; Park, B.; Goel, A.; Aggarwal, B. B. *Genes Nutr.* **2011**, *6*, 93−108.

(27) Teiten, M.-H.; Dicato, M.; Diederich, M. *Mol. Nutr. Food Res.* **2013**, *57*, 1619−1629.

(28) Chen, Y.; Shu, W.; Chen, W.; Wu, Q.; Liu, H.; Cui, G. *Basic Clin. Pharmacol. Toxicol.* **2007**, *101*, 427−433.

(29) Liu, H. L.; Chen, Y.; Cui, C. H.; Zhou, J. F. *Acta Pharmacol. Sin.* **2005**, *26*, 603−609.

(30) Wu, Q.; Chen, Y.; Li, X. *J. Huazhong Univ. Sci. Technol., Med. Sci.* **2006**, *26*, 199−210.

(31) Shu, L.; Khor, T. O.; Lee, J.-H.; Boyanapalli, S. S. S.; Huang, Y.; Wu, T.-Y.; Saw, C. L. L.; Cheung, K.-L.; Kong, A.-N. T. *AAPS J.* **2011**, *13*, 606−614.

(32) Lin, K.-T.; Wang, Y.-W.; Chen, C.-T.; Ho, C.-M.; Su, W.-H.; Jou, Y.-S. *Clin. Cancer Res.* **2012**, *18*, 4691−4701.

(33) Chang, H.-H.; Meuillet, E. J. *Future Med. Chem.* **2011**, *3*, 1909−1934.

(34) Funk, C. D. *Science* **2001**, *294*, 1871−1875.

(35) Claveau, D.; Sirinyan, M.; Guay, J.; Gordon, R.; Chan, C. C.; Bureau, Y.; Riendeau, D.; Mancini, J. A. *J. Immunol.* **2003**, *170*, 4738−4744.

(36) Kojima, F.; Naraba, H.; Miyamoto, S.; Beppu, M.; Aoki, H.; Kawai, S. *Arthritis Res. Ther.* **2004**, *6*, R355−R365.

(37) Masuko-Hongo, K.; Berenbaum, F.; Humbert, L.; Salvat, C.; Goldring, M. B.; Thirion, S. *Arthritis Rheum.* **2004**, *50*, 2829−2838.

(38) Li, X. F.; Afif, H.; Cheng, S.; Martel-Pelletier, J.; Pelletier, J. P.; Ranger, P.; Fahmi, H. *J. Rheumatol.* **2005**, *32*, 887−895.

(39) Subbaramaiah, K.; Yoshimatsu, K.; Scherl, E.; Das, K. M.; Glazier, K. D.; Golijanin, D.; Soslow, R. A.; Tanabe, T.; Naraba, H.; Dannenberg, A. J. *J. Biol. Chem.* **2004**, *279*, 12647−12658.

(40) Nakanishi, M.; Montrose, D. C.; Clark, P.; Nambiar, P. R.; Belinsky, G. S.; Claffey, K. P.; Xu, D.; Rosenberg, D. W. *Cancer Res.* **2008**, *68*, 3251−3259.

(41) Wiegard, A.; Hanekamp, W.; Griessbach, K.; Fabian, J.; Lehr, M. *Eur. J. Med. Chem.* **2012**, *48*, 153−163.

(42) Roersch, F.; Wobst, I.; Zettl, H.; Schubert-Zsilavecz, M.; Groesch, S.; Geisslinger, G.; Schneider, G.; Proschak, E. *J. Med. Chem.* **2010**, *53*, 911−915.

(43) Shiro, T.; Takahashi, H.; Kakiguchi, K.; Inoue, Y.; Masuda, K.; Nagata, H.; Tobe, M. *Bioorg. Med. Chem. Lett.* **2012**, *22*, 285−288.

(44) Bauer, J.; Koeberle, A.; Dehm, F.; Pollastro, F.; Appendino, G.; Northoff, H.; Rossi, A.; Sautebin, L.; Werz, O. *Biochem. Pharmacol.* **2011**, *81*, 259−268.

(45) Koeberle, A.; Rossi, A.; Zettl, H.; Pergola, C.; Dehm, F.; Bauer, J.; Greiner, C.; Reckel, S.; Hoernig, C.; Northoff, H.; Bernhard, F.; Doetsch, V.; Sautebin, L.; Schubert-Zsilavecz, M.; Werz, O. *J. Pharmacol. Exp. Ther.* **2010**, *332*, 840−848.

(46) Norberg, J. K.; Sells, E.; Chang, H.-H.; Alla, S. R.; Zhang, S.; Meuillet, E. J. *Pharm. Pat. Anal.* **2013**, *2*, 265−288.

DOI: 10.1021/acs.jnatprod.5b00700
J. Nat. Prod. XXXX, XXX, XXX−XXX

(47) Sjogren, T.; Nord, J.; Ek, M.; Johansson, P.; Liu, G.; Geschwindner, S. *Proc. Natl. Acad. Sci. U. S. A.* **2013**, *110*, 3806−3811.
(48) Luz, J. G.; Antonysamy, S.; Kuklish, S. L.; Condon, B.; Lee, M. R.; Allison, D.; Yu, X. P.; Chandrasekhar, S.; Backer, R.; Zhang, A.; Russell, M.; Chang, S. S.; Harvey, A.; Sloan, A. V.; Fisher, M. J. *J. Med. Chem.* **2015**, *58*, 4727−4737.
(49) Li, D.; Howe, N.; Dukkipati, A.; Shah, S. T. A.; Bax, B. D.; Edge, C.; Bridges, A.; Hardwicke, P.; Singh, O. M. P.; Giblin, G.; Pautsch, A.; Pfau, R.; Schnapp, G.; Wang, M.; Olieric, V.; Caffrey, M. *Cryst. Growth Des.* **2014**, *14*, 2034−2047.
(50) Genovese, S.; Curini, M.; Epifano, F. *Phytochemistry* **2009**, *70*, 1082−1091.
(51) Epifano, F.; Genovese, S.; Menghini, L.; Curini, M. *Phytochemistry* **2007**, *68*, 939−953.
(52) Marcu, M. G.; Jung, Y.-J.; Lee, S.; Chung, E.-J.; Lee, M.-J.; Trepel, J.; Neckers, L. *Med. Chem.* **2006**, *2*, 169−174.
(53) Liu, Z.; Xie, Z.; Jones, W.; Pavlovicz, R. E.; Liu, S.; Yu, J.; Li, P.-k.; Lin, J.; Fuchs, J. R.; Marcucci, G.; Li, C.; Chan, K. K. *Bioorg. Med. Chem. Lett.* **2009**, *19*, 706−709.
(54) Avonto, C.; Taglialatela-Scafati, O.; Pollastro, F.; Minassi, A.; Di Marzo, V.; De Petrocellis, L.; Appendino, G. *Angew. Chem., Int. Ed.* **2011**, *50*, 467−471.
(55) *Glide* Version 6.1; Schrödinger, LLC: New York, NY, 2013.
(56) Halgren, T. A.; Murphy, R. B.; Friesner, R. A.; Beard, H. S.; Frye, L. L.; Pollard, W. T.; Banks, J. L. *J. Med. Chem.* **2004**, *47*, 1750−1759.
(57) Friesner, R. A.; Banks, J. L.; Murphy, R. B.; Halgren, T. A.; Klicic, J. J.; Mainz, D. T.; Repasky, M. P.; Knoll, E. H.; Shelley, M.; Perry, J. K.; Shaw, D. E.; Francis, P.; Shenkin, P. S. *J. Med. Chem.* **2004**, *47*, 1739−1749.
(58) Friesner, R. A.; Murphy, R. B.; Repasky, M. P.; Frye, L. L.; Greenwood, J. R.; Halgren, T. A.; Sanschagrin, P. C.; Mainz, D. T. *J. Med. Chem.* **2006**, *49*, 6177−6196.
(59) Millard, C. J.; Watson, P. J.; Celardo, I.; Gordiyenko, Y.; Cowley, S. M.; Robinson, C. V.; Fairall, L.; Schwabe, J. W. R. *Mol. Cell* **2013**, *51*, 57−67.
(60) Bressi, J. C.; Jennings, A. J.; Skene, R.; Wu, Y.; Melkus, R.; De Jong, R.; O'Connell, S.; Grimshaw, C. E.; Navre, M.; Gangloff, A. R. *Bioorg. Med. Chem. Lett.* **2010**, *20*, 3142−3145.
(61) Watson, P. J.; Fairall, L.; Santos, G. M.; Schwabe, J. W. R. *Nature* **2012**, *481*, 335−340.
(62) Somoza, J. R.; Skene, R. J.; Katz, B. A.; Mol, C.; Ho, J. D.; Jennings, A. J.; Luong, C.; Arvai, A.; Buggy, J. J.; Chi, E.; Tang, J.; Sang, B. C.; Verner, E.; Wynands, R.; Leahy, E. M.; Dougan, D. R.; Snell, G.; Navre, M.; Knuth, M. W.; Swanson, R. V.; McRee, D. E.; Tari, L. W. *Structure* **2004**, *12*, 1325−1334.
(63) Bottomley, M. J.; Lo Surdo, P.; Di Giovine, P.; Cirillo, A.; Scarpelli, R.; Ferrigno, F.; Jones, P.; Neddermann, P.; De Francesco, R.; Steinkuhler, C.; Gallinari, P.; Carfi, A. *J. Biol. Chem.* **2008**, *283*, 26694−26704.
(64) Schuetz, A.; Min, J.; Allali-Hassani, A.; Schapira, M.; Shuen, M.; Loppnau, P.; Mazitschek, R.; Kwiatkowski, N. P.; Lewis, T. A.; Maglathin, R. L.; McLean, T. H.; Bochkarev, A.; Plotnikov, A. N.; Vedadi, M.; Arrowsmith, C. H. *J. Biol. Chem.* **2008**, *283*, 11355−11363.
(65) Bieliauskas, A. V.; Pflum, M. K. H. *Chem. Soc. Rev.* **2008**, *37*, 1402−1413.
(66) Thaler, F.; Mercurio, C. *ChemMedChem* **2014**, *9*, 523−536.
(67) Askari, M.; Sahebkar, A.; Iranshahi, M. *Iran J. Basic Med. Sci.* **2009**, *12*, 63−69.
(68) Koeberle, A.; Siemoneit, U.; Buehring, U.; Northoff, H.; Laufer, S.; Albrecht, W.; Werz, O. *J. Pharmacol. Exp. Ther.* **2008**, *326*, 975−982.
(69) Covalent Docking, protocol 2013-3. *Glide* Version 6.1, Prime Version 3.4; Schrödinger, LLC: New York, NY, 2013.
(70) Peret-Almeida, L.; Cherubino, A. P. F.; Alves, R. J.; Dufosse, L.; Gloria, M. B. A. *Food Res. Int.* **2005**, *38*, 1039−1044.
(71) *Maestro*, Version 9.6; Schrödinger, LLC: New York, NY, 2013.
(72) *LigPrep*, Version 2.8; Schrödinger, LLC: New York, NY, 2013.
(73) Schrodinger Software Release 2013-3; Schrödinger LLC, New York, NY, 2013.

DOI: 10.1021/acs.jnatprod.5b00700
J. Nat. Prod. XXXX, XXX, XXX−XXX